Enfuvirtide-Protoporphyrin IX Dual-Loaded Liposomes: In Vitro Evidence of Synergy against HIV-1 Entry into Cells

Tiago Figueira, Marco Domingues, Françoise Illien, Iris Cadima-Couto, Toni Todorovski, David Andreu, Sandrine Sagan, Miguel Castanho, Astrid Walrant, Ana Salomé Veiga

Enfuvirtide-protoporphyrin IX dual-loaded liposomes: *in vitro* evidence of synergy against HIV-1 entry into cells

Tiago N. Figueira[1], Marco M. Domingues[1], Françoise Illien[2], Iris Cadima-Couto[1], Toni Todorovski[3], David Andreu[3], Sandrine Sagan[2], Miguel A.R.B. Castanho[1], Astrid Walrant[2]*, Ana Salomé Veiga[1]*

[1]*Instituto de Medicina Molecular, Faculdade de Medicina, Universidade de Lisboa, 1649-028 Lisbon, Portugal*
[2]*Sorbonne Université, École normale supérieure, PSL University, CNRS, Laboratoire des Biomolécules, LBM, 75005 Paris, France*
[3]*Department of Experimental and Health Science, Universitat Pompeu Fabra, Barcelona Biomedical Research Park, 08003 Barcelona, Spain*

*Correspondence to: Ana Salomé Veiga and Astrid Walrant (e-mails: aveiga@medicina.ulisboa.pt and astrid.walrant@sorbonne-universite.fr)

Abstract

We have developed a nanocarrier consisting of large unilamellar vesicles (LUVs) for combined delivery of two human immunodeficiency virus type 1 (HIV-1) entry inhibitors, enfuvirtide (ENF) and protoporphyrin IX (PPIX). The intrinsic lipophilicity of ENF and PPIX, a fusion inhibitor and an attachment inhibitor, respectively, leads to their spontaneous incorporation into the lipid bilayer of the LUVs nanocarrier. Both entry inhibitors partition significantly towards LUVs composed of 1-palmitoyl-2-oleoyl-*sn*-glycero-3-phosphocholine (POPC) and a 9:1 mixture of POPC:1,2-dipalmitoyl-*sn*-glycero-3-phosphoethanolamine-*N*-[methoxy(polyethylene glycol)-2000] (DPPE-PEG_{2000}), representative of conventional and immune-evasive drug delivery formulations, respectively. These co-localize in the core of lipid membranes. Dual-loaded nanocarriers are monodispersed and retain the size distribution, membrane fluidity, and surface charge of the unloaded form. Combination of the two entry inhibitors in the nanocarrier resulted in improved synergy against HIV-1 entry compared to combination in free form, strongly when immune-evasive formulations are used. We propose that the improved action of the entry inhibitors when loaded into the nanocarriers results from their slow release at the site of viral entry. Overall, liposomes remain largely unexplored platforms for combination of viral entry inhibitors, with potential for improvement of current antiretroviral therapy drug safety and application. Our work calls for a reappraisal of the potential of entry inhibitors combinations and delivery for clinical use in antiretroviral therapy.

Keywords: HIV, entry, inhibitor, liposome, membrane, nanocarrier, delivery

Introduction

Human immunodeficiency virus type 1 (HIV-1) entry into host immune cells results from the complex interplay between the viral envelope glycoproteins (Env), cellular receptors and co-receptors, and lipid membranes.[1] Env, a key player in this process, consists of a heterodimeric ensemble of gp120 (peripheral) and gp41 (transmembrane) protein homotrimers, non-covalently associated in heavily glycosylated metastable complexes.[2] Both subunits participate in the multi-step entry process though with independent functions; gp120 mediates binding to CD4 receptors and docking to CCR5 or CXCR4 co-receptors, while gp41 inserts into target cell lipid membranes, leading to conformational-dependent membrane approximation, lipid mixing and fusion.[3] Entry inhibitors, one of the antiretroviral drug classes in clinical use against HIV-1, target early stages of infection, prior to viral entry into cells.[4] The mechanism may consist in preventing efficacious virion attachment to cells,[5] either by inhibiting receptor or co-receptor docking,[6] or blocking the conformational transitions required for membranes fusion.[7] New entry inhibitor drug candidates frequently fail during clinical trials[8,9] due to high associated costs,[10] undesirable side effects[11] and suboptimal pharmacokinetic performance,[12] namely low solubility, short half-life, slow absorption and/or low bioavailability.

In principle, the pharmacokinetics and safety profiles of entry inhibitors would benefit from alternative drug delivery and targeting strategies, using soft-matter nanocarrier devices. Recently, liposomes have been suggested as potential scaffolds for nanocarriers of HIV-1 antiretrovirals,[13] particularly for entry inhibitors delivery.[14] Current liposome technology has achieved highly stable formulations, such as immune-evasive liposomes,[15] capable of efficient delivery through blood and lymphatic circulation, while avoiding extensive immune system-mediated elimination.[16] Lipids can be fine-tuned and chemically modified to provide compatible design-function relationships, tailored for stable loading, targeted delivery and stimuli-responsive controlled release.[17] Through this, liposomes can improve the efficacy and safety profiles of multiple drugs, reducing clearance levels, off-target effects and toxicity. As a result, numerous liposome-based formulations have obtained approval for clinical use, though few have been successfully designed for anti-HIV-1 therapy.[18] Despite the potential of liposomes as carriers for antiretroviral drug combinations, these remain largely unexplored in the context of antiretroviral delivery and synergy.

Several Env-targeting entry inhibitors share a common high affinity towards lipid membranes. Entry inhibitor-lipid membrane interactions are well described in the literature and correlate with entry inhibitors efficacy.[19-22] Enfuvirtide (ENF), a fusion inhibitor peptide,[23] and protoporphyrin IX (PPIX), a small molecule targeting the Env V3 loop-CD4 binding,[24] are known for their ability to extensively interact with zwitterionic lipid membranes.[19,24] To take advantage of this property, we opted for incorporation within liposomes membranes instead of a common encapsulation strategy, such as the one described for antimicrobial amphotericin B-loaded liposomes (AmBisome®).[25] This provides fundamental advantages for PPIX solubility, which is low in polar solvents but high in organic amphipathic solvents such as DMSO. Additionally, the ENF α-helix interfacial hydrophobicity associated with membrane adsorption and partition is also a determinant of gp41 binding, modulated by peptide secondary structure content in both environments.[19,22] Further advantages were found in

applying immune-evasive liposomes compositions, exposing hydrophilic coatings from PEG-derivatized lipids, as an alternative to conventional bare liposomes.[15] While conventional liposomes are susceptible to protein opsonization and subsequent systemic elimination, immune-evasive PEG-coated liposomes are expected to prolong circulation times, protecting membrane associated cargo.[26,27] In the present work, we explore how these clinically-relevant entry inhibitors can be loaded into liposome nanocarriers, either independently or in combination, with a focus on dual-delivery and synergistic HIV-1 entry inhibition. Considering that ENF is approved for antiretroviral therapy and PPIX has multiple applications in the clinic,[28,29] our proposed nanocarrier represents a promising proof-of-concept for improved therapeutic entry inhibitors drug delivery.

Results and Discussion

ENF and PPIX have synergistic activity against HIV-1 entry

The effectiveness of drugs combinations used in antiretroviral therapy regimens are dependent on advantageous drug-drug interactions, *i.e.* synergy.[30,31] ENF targets the gp41 pre-fusion conformation and prevents the conformational transitions required for viral fusion pore formation.[23] On the other hand, PPIX is known to bind to gp120 domains relevant for CD4 recognition, but its mode of action is not yet fully understood.[32,33] For instance, PPIX photodynamic properties do not correlate with increased HIV-1 inactivation,[34] as observed for other viruses.[24] Therefore, we first questioned if ENF and PPIX act on different steps of the viral entry, thus not competing for the same target. For this purpose, we studied the efficacy of each entry inhibitor against HIV-1 laboratory-adapted strain NL4-3 (HIV-1_{NL4-3}) entry into TZM-bl cells, at different moments of the viral entry process, by varying the time of entry inhibitors addition *in vitro* (Fig. S2 and 1, A). Both entry inhibitors were most effective when pre-incubated or added simultaneously with HIV-1_{NL4-3} to cells. Pre-incubation of HIV-1_{NL4-3} viruses with either ENF or PPIX, for 1 h, did not improve virus inactivation when compared to simultaneous addition. ENF showed a gradual decrease in effectiveness when added 1 h or later after virus addition, becoming totally ineffective when added 3 h post-infection. PPIX was totally ineffective when added 1 h or later post-infection, such as observed with the attachment inhibitor dextran sulfate (DEX). Our results are consistent with PPIX acting upon the initial Env gp120-CD4 recognition, whereas ENF blocks the gp41-mediated fusion, which occurs afterwards. PPIX antiretroviral properties were not dependent on photoactivation, as suggested in previous studies.[34] This is favorable for our liposomal nanocarrier system, since porphyrin photoactivation is known to disrupt lipid bilayer structures. PPIX applications, as well as metal derivatives, may also have potential for viral co-infection treatment since they show antiviral properties against Dengue, Yellow Fever and Vesicular Stomatitis viruses, with complementary modes-of-action.[24,35]

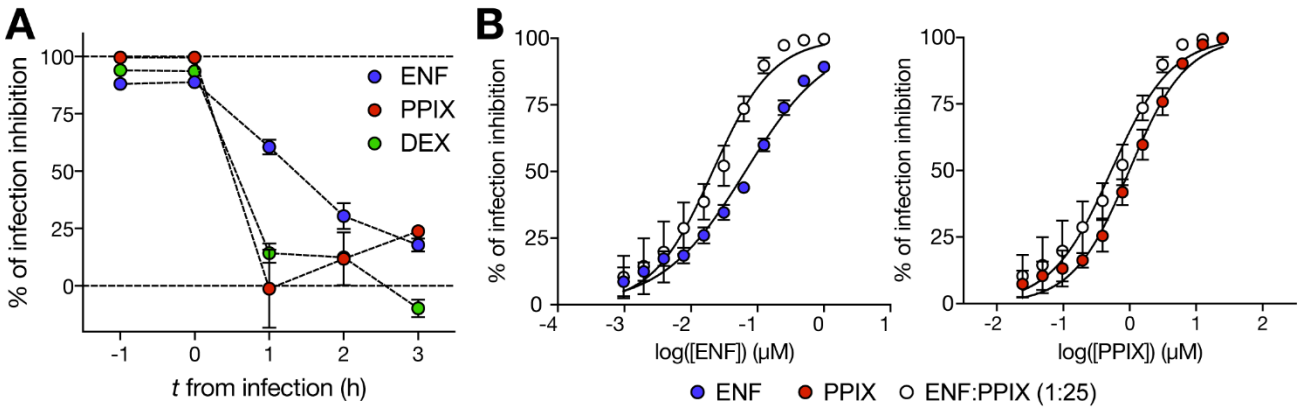

Figure 1 – *In vitro* evaluation of ENF and PPIX time-of-action and efficacy against HIV-1 entry. (A) Effect of time-of-inhibitor-addition on ENF (1 μM), PPIX (25 μM) and DEX (0.5 μM) efficacy against HIV-1_{NL4-3} entry into TZM-bl cells. TZM-bl cells were treated with each entry inhibitor at -1 h, 0 h, +1 h, +2 h or +3 h relatively to the moment of HIV-1_{NL4-3} virus addition (100 $TCID_{50}$). The presented % of infection inhibition values were taken from the respective dose-response curves, at the maximum entry inhibitors concentration tested (Fig. S2). **(B)** Dose-response curves of ENF, PPIX, and ENF:PPIX (1:25) combination against HIV-1_{NL4-3} entry into TZM-bl cells. entry inhibitors were added simultaneously with HIV-1_{NL4-3} (100 $TCID_{50}$) to TZM-bl cells. Viral infectivity was quantified 48 h post-infection through luciferase reporter-enzyme activity and converted to viral inhibition using Eq. 4 and 5. Results correspond to the average of three independent experiments.

Since virus attachment and fusion are sequential steps of the HIV entry mechanism, associated with different target glycoproteins,[36,37] we further tested if ENF and PPIX have synergistic activity against HIV-1_{NL4-3} entry, when combined in aqueous solution. Thus, we compared the efficacy of each entry inhibitor separately to the efficacy of a ENF:PPIX (1:25) combination, simultaneously added with viruses to cells *in vitro* (Fig. 1, B). Cell culture viability in the presence of each entry inhibitor and combinations was assessed, in parallel. Entry inhibitors combination lowered the IC_{50} of ENF from 65.8 nM to 21.3 nM and of PPIX from 987.8 nM to 531.4 nM (Table 1). Both ENF and PPIX were non-cytotoxic under the same assay conditions (Fig. S3). In order to understand if the observed effect was the result of synergy, we performed a combined comparative and quantitative analysis of the combination dose-response data (Fig. S4). Both the Bliss Independence and the Loewe Additivity models were used as reference for the comparative analysis. These models make use of the individual performance of each entry inhibitor to predict the additive efficacy of their combination, independently of any synergistic effects. Because their assumptions differ, the models provide complementing thresholds for comparison with the experimental data in order to evaluate synergy (Supporting Information, Section 1). The median-effects plot for the ENF:PPIX combination overlapped with the Bliss Independence model and showed a relative positive inflection at high concentrations when compared to the Loewe Additivity model, suggesting low-moderate synergism (Fig. S4, A). Since both ENF and PPIX act upon the Env complex, at the level of viral entry, their combined effect was not expected to overcome the predicted Bliss effect.[31,38]

Combination index (CI) values, determined through the Chou-Talalay quantitative method, also suggest entry inhibitors synergism at concentrations above the IC_{50}, as demonstrated by CI values below 1 (Fig. S4, B). In both analysis, synergism was dose dependent, *i.e.* evident at entry inhibitors concentrations inducing more potent inhibition.

According to the literature, ENF shows higher synergy with maraviroc (MVC) and AMD3100, respectively, CCR5 and CXCR4 antagonist entry inhibitors, compared to PPIX.[31,36] Even though both compounds inhibit the HIV-1 entry, neither MVC nor AMD3100 act on the viral Env complex. These bind to endogenous cell co-receptors,[39,40] which may contribute to the apparent differences in synergistic potential relative to PPIX. Nonetheless, PPIX can broadly impact HIV-1 CD4 attachment independently of viral co-receptor tropism, while MVC and AMD3100 application is specific towards R5 or X4 viruses, respectively, in independent stages of systemic infection. It is also relevant to consider potential differences resulting from the combination of molecular ratios between the respective entry inhibitors.

Table 1 – IC_{50} of ENF and PPIX alone and in combination against HIV-1_{NL4-3} entry *in vitro.* In the case of combined administration of ENF:PPIX, the columns ENF and PPIX pertain to the concentration of the component in the mixture.

	Formulation	IC_{50} (± *SD* nM)	
		ENF	**PPIX**
individual	aqueous solution	65.8 (±6.9)	987.8 (±105.9)
	POPC[a]	81.2 (±15.4)	1422 (±275.9)
	POPC:DPPE-PEG_{2000} (9:1)[a]	27.2 (±5.3)	484.0 (±41.8)
combined ENF:PPIX (1:25)	aqueous solution	21.3 (±3.3)	531.4 (±141.9)
	POPC[a]	19.7 (±3.8)	491.8 (±94.8)
	POPC:DPPE-PEG_{2000} (9:1)[a]	10.4 (±1.3)	259.0 (±16.7)

[a] Lipid concentration was 500 μM.

ENF and PPIX co-partition into the core of lipid bilayers in liposomes

ENF shows high affinity towards 1-palmitoyl-2-oleoyl-*sn*-glycero-3-phosphocholine (POPC),[19] an approved lipid for clinical use.[41] We questioned whether PPIX would have similar behavior, establishing POPC as a possible lipid scaffold for dual-loading of ENF and PPIX. Using the intrinsic fluorescence emission of both entry inhibitors, we monitored partition towards POPC LUVs membranes (Fig. 2, A and B). In addition, an immune-evasive formulation composed of a 9:1 mixture of POPC and 1,2-dipalmitoyl-*sn*-glycero-3-phosphoethanolamine-*N*-[methoxy(polyethylene glycol)-2000] (DPPE-PEG_{2000}) was also studied. PPIX shows considerable partition towards POPC and POPC:DPPE-PEG_{2000} LUVs membranes, as portrayed by the respective partition constants (K_p) values of 3.07 x 10^3 and 3.98 x 10^3 (Table 2). ENF also partitions towards LUVs membranes with both lipid compositions, with K_p values of 1.18 x 10^3 and 0.92 x 10^3, respectively (Table 2). According to the entry inhibitor time-resolved fluorescence emission profiles, the partition equilibrium is reached within 10 min for both ENF and PPIX upon addition of LUVs (Fig. S5). The high order of magnitude

of the K_p values associated with each entry inhibitor suggest that the partition equilibrium will be substantially shifted towards membrane incorporation and accumulation. PEG-coated liposomes had already been suggested as suitable carriers for lipophilic porphyrins since these seem to be stabilized by the polymer coating.[42] Even though the PEG mesh coating prevents protein adhesion to the membrane surface, it still allows penetration of small molecules and peptides. As the system depends on entry inhibitors partition towards lipid membranes for effective loading, it also depends on the impact of environmental factors on the partition equilibrium for release from the membrane at the site of action,[43,44] such as the equilibrium shifts due to entry inhibitors incorporation into cell membranes, or liposome internalization or degradation. Since these compounds accumulate in the outer leaflet of the liposomes lipid bilayer, they are released to the extracellular space even in the event of liposome fusion with cells plasma membrane, becoming bioavailable near their site of action.

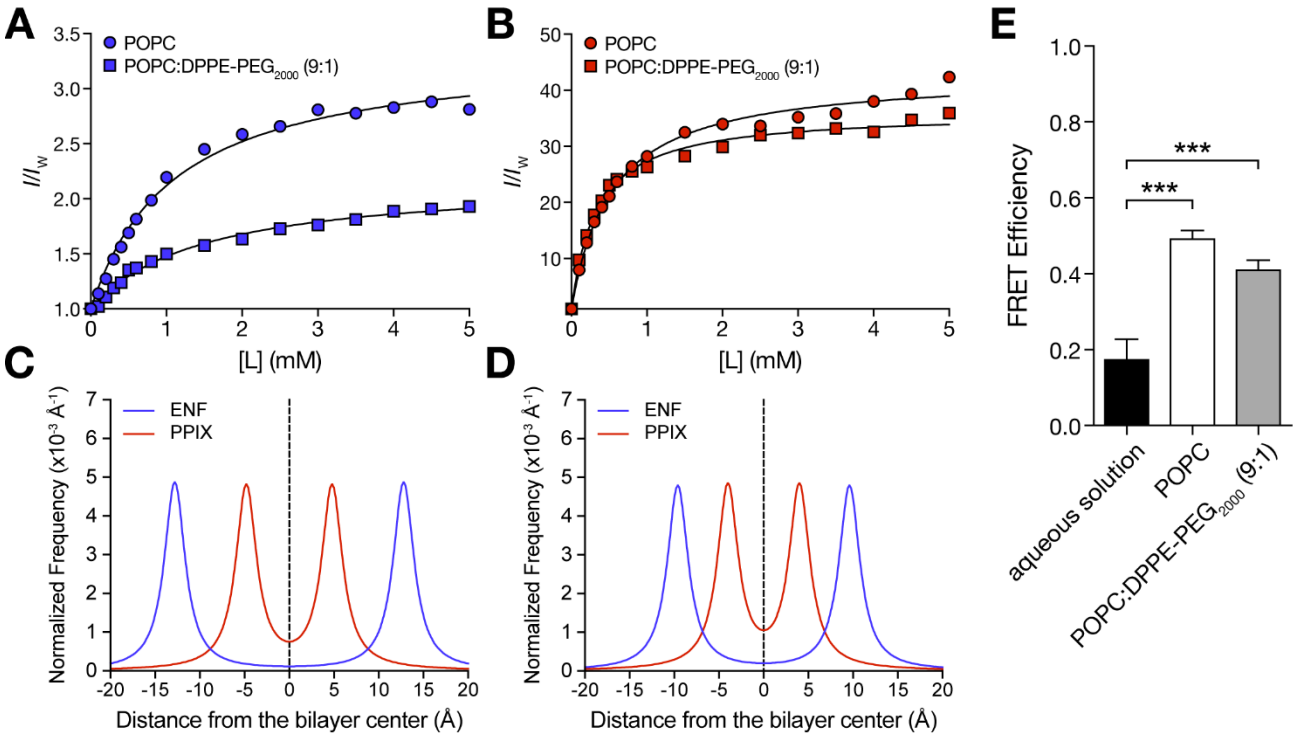

Figure 2 – Biophysical characterization of ENF and PPIX interaction with LUVs membranes. (A and B) Partition of ENF (A) and PPIX (B) towards POPC and POPC:DPPE-PEG$_{2000}$ (9:1) LUVs membranes. Partition profiles of ENF and PPIX (10 μM) were followed by Trp or intrinsic fluorescence emission, respectively, at increasing lipid concentrations. Lines correspond to the best fit of Eq. 1 to the experimental data. Results correspond to one of three independent replicates. **(C and D)** Intra-membrane depth localization of ENF and PPIX (10 μM) within POPC (C) and POPC:DPPE-PEG$_{2000}$ (9:1) (D) LUVs membranes. Lipid bilayer penetration depth histograms of fluorophores were estimated through differential fluorescence emission quenching with lipophilic 5-NS and 16-NS (Fig. S6), in the presence of liposomes (3 mM). Results correspond one of three independent replicates. **(E)** Co-localization of ENF and PPIX in aqueous solution and within POPC and POPC:DPPE-PEG$_{2000}$ (9:1) LUVs membranes. FRET efficiency between ENF and PPIX was quantified

through Trp fluorescence emission, in the absence or presence of LUVs (200 μM), using Eq. 3. Results correspond to the average of three independent experiments. *** – $P \leq 0.001$.

Table 2 – K_p of ENF and PPIX towards LUVs membranes

	K_p x 10^3 (±*SD*)	
Formulation	**ENF**	**PPIX**
POPC	1.18 (±0.09)	3.07 (±0.57)
POPC:DPPE-PEG_{2000} (9:1)	0.92 (±0.19)	3.98 (±0.03)

Although both entry inhibitors partition towards the studied LUVs, they may compete for loading space in the membrane, reducing the transportation effectiveness of the entry inhibitor-LUV (EI-LUV) nanocarrier system. We probed the entry inhibitors penetration depth into POPC and POPC:DPPE-PEG_{2000} lipid bilayers in LUVs through a differential entry inhibitors fluorescence emission quenching approach. Lipophilic quenchers 5-doxyl stearic acid (5-NS) and 16-doxyl stearic acid (16-NS) located at the bilayer interface and center regions, respectively, were used to estimate the respective entry inhibitors intra-membrane depth localization (Fig. 2, C and D; Fig. S6). ENF tryptophan residues (Trp) were found to locate closer to the bilayer interface, at 12.8 and 9.6 Å from the bilayer center in POPC and POPC:DPPE-PEG_{2000} LUVs, respectively. This is a trend followed by other gp120-derived fusion inhibitor peptides[20,45] and is in agreement with previous reports in the literature.[19] Since ENF Trp are located closer to the C-terminus, the peptide may assume a slightly tilted inserted position as predicted for other membrane-active peptides.[46] PPIX was predicted to be buried within membranes, at approximately 4.8 and 4.0 Å from the bilayer center in POPC and POPC:DPPE-PEG_{2000} LUV, respectively. Quenching by the 5-NS quencher was undetectable in this case (Fig. S6). PPIX is expected to fully insert within highly hydrophobic environments,[42] orienting its carboxyl groups towards the lipid polar heads. Thus, ENF and PPIX insert in lipid bilayers but have minimal overlap, therefore being potentially competent for simultaneous loading into LUVs, independently of the PEG coating.

To evaluate if both entry inhibitors can indeed be simultaneously loaded into LUVs, we monitored ENF and PPIX co-localization within membranes using a Förster Resonance Energy Transfer (FRET)-based fluorescence spectroscopy approach (Fig. 2, E). FRET efficiency correlates with the proximity between donor and acceptor fluorophores. The FRET efficiency between entry inhibitors in aqueous solution was 0.17, which we assign to a basal level of PPIX aggregation,[47] facilitating contact between donor and acceptor fluorophores. When incubated with either POPC or POPC:DPPE-PEG_{2000} LUVs, the FRET efficiency increased to 0.49 and 0.41, respectively. Such an increase in FRET efficiency suggests that the distance between ENF and PPIX is reduced as a result of co-partitioning towards the same membranes. This further supports the compatibility of both conventional and immune-evasive LUVs formulations for entry inhibitors dual-loading and respective antiretroviral applications.

EI-LUV nanocarriers are stable in solution

The pharmacokinetic advantages of liposomes for nanocarrier drug delivery applications rely on colloidal stability, especially if the therapeutic molecules are loaded at the membrane-level,[48] which is the case in this study. Most clinically approved liposomes formulations have diameters between 50 and 300 nm. We opted for POPC LUVs extruded through polycarbonate membrane filters with 100 nm pore size, which are suitable for *in vivo* applications; they evade the mononuclear phagocyte system and maximize entry inhibitors partition.[49] Depending on the affinity towards the lipid phase and respective chemistry, small molecules and peptides may induce LUVs aggregation, lipid mixing and/or disruption, which are undesireable for drug delivery applications.[50,51] LUVs average hydrodynamic diameter (D_H), polydispersity index (PDI) and ζ-potential were quantified through dynamic light scattering (DLS) and used as a measure of stability (Fig. 3, A-C; Fig. S7). Unloaded POPC and POPC:DPPE-PEG_{2000} (9:1) LUVs were monodispersed (PDI~0.1) and zwitterionic, with a D_H between 110 and 130 nm, respectively. Both entry inhibitors were combined with LUVs at concentrations relevant for *in vitro* experimentation, generating single- or dual-loaded EI-LUV nanocarriers. ENF single-loading into LUVs membranes did not significantly change their biophysical properties of size and charge (Fig. S7). In contrast, upon PPIX single-loading, LUVs of both lipid compositions showed a slight increase in D_H, without significant impact on the intensity-averaged size distribution (Fig. S6). This was complemented by an increase in PDI and decrease in ζ-potential of PPIX-loaded EI-LUV. The PEG coating of immune-evasive LUVs prevented the PPIX-associated decrease in ζ-potential. When both entry inhibitors were combined in LUVs, their biophysical properties, as size and charge, were predominantly affected by PPIX, as expected from independent experiments with each entry inhibitor (Fig. 3, A-C). In all cases, LUVs maintained PDI values below 0.3, which is within acceptable values for monodisperse systems.[52] It is relevant to acknowledge that entry inhibitors did not disrupt the LUVs membrane integrity, even at relevant inhibitory concentrations. Importantly, system stability seems to depend on a balance between the entry inhibitor/lipid ratio which can be easily regulated by increasing/decreasing one of these components (Fig. 3 and S7). ENF, for instance, was predicted to saturate in POPC membranes at a 1/50 peptide/lipid ratio,[44] with negligible effect on membrane stability. Such observations are encouraging for further applications in more challenging *in vivo* environments.

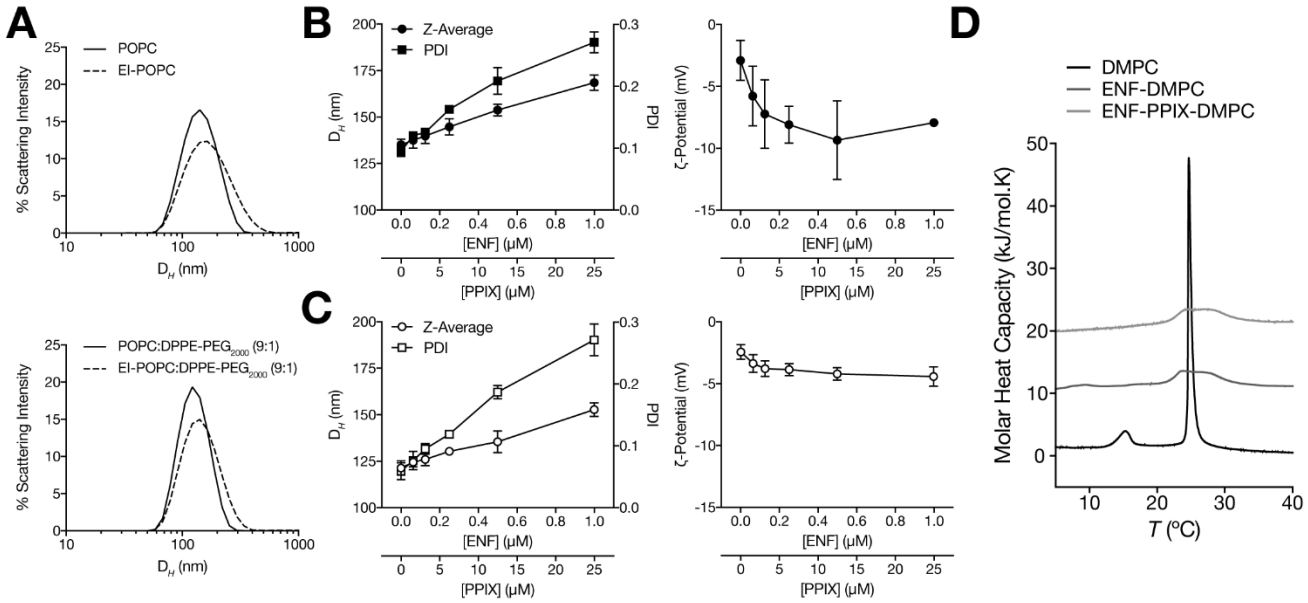

Figure 3 - Effect of entry inhibitors dual-loading on zwitterionic (POPC, POPC:DPPE-PEG$_{2000}$ or DMPC) lipid vesicles properties and colloidal stability. (A) Representative intensity-averaged size distribution histograms of POPC (top) or POPC:DPPE-PEG$_{2000}$ (9:1) (bottom) LUVs (500 μM) dual-loaded with PPIX (25 μM) and ENF (1 μM). Unloaded LUVs are presented as a control. **(B and C)** D_H, PDI (left) and ζ-potential (right) of dual-loaded POPC (B) and POPC:DPPE-PEG$_{2000}$ (9:1) (C) EI-LUV (500 μM). LUVs were loaded with ENF:PPIX (1:25) combination, at increasing entry inhibitors concentrations. Results correspond to the average of at least three independent experiments. **(D)** DSC profiles of DMPC multilamellar vesicles (1 mg/mL) single-loaded with ENF and dual-loaded with both ENF and PPIX. ENF and PPIX were incubated with multilamellar vesicles at 1/50 and 1/10 molar ratios relatively to the final lipid concentration, respectively. Unloaded multilamellar vesicles are presented as a control. Results correspond to one of two independent replicates.

Assessing the effect of the addition of ENF and PPIX on the membrane fluidity is also important, as it can influence liposomes deformability and tissue penetration.[53,54] To further complement our analysis, we questioned whether entry inhibitors incorporation into lipid membranes would have an impact on the lipid membrane phase behavior. Differential scanning calorimetry (DSC) was used to quantify lipid phase transition temperature variations (Fig. 3, D); 1,2-dimyristoyl-*sn*-glycero-3-phosphocholine (DMPC) membranes were used, due to the technical limitations associated to the low T_m of POPC membranes (~ -2ºC). DMPC multilamellar vesicles have a T_{pre} of 15.1 ºC and T_m of 24.6 ºC (Table 3). Addition of ENF alone led to a large modification of the transition peaks. The pre-transition is dampened, almost disappearing. The main transition is also strongly affected, with a large broadening of the peak and a decrease in transition enthalpy, suggesting efficient insertion of ENF in the bilayer, as reported for POPC. Splitting of the transition peak is likely due to lateral segregation in the bilayer. The broad transition peak can be deconvoluted into two components. The low temperature component (T_{m1} = 23.6 °C; slight stabilization of the fluid phase) contributing for 16 % of the total

transition enthalpy corresponds to regions where DMPC is little affected by the presence of ENF. The high temperature component (T_{m2} = 27.1 °C) corresponds to regions where ENF is enriched and strongly affects DMPC, with a tendency to destabilize the fluid phase. When ENF and PPIX were combined, the transition peak is similarly affected. This suggests that both entry inhibitors interact with the surface and the core of the membrane and lead to membrane fluidification in contrast to ENF alone. The ENF:PPIX molar ratio was adjusted to 1:5 in this case to avoid excessive DMSO concentrations in samples, which could impact the integrity and stability of liposomes.[55,56] Altogether, ENF and PPIX insert in the bilayer of DMPC multilamellar vesicles and lead to lateral segregation in the bilayer. In the presence of PPIX, the more rigid region is slightly less stabilized than with ENF alone. It should be stressed that although ENF slightly destabilizes the fluid phase, other studies showed that it has higher affinity towards fluid phase membranes and may benefit from dual-loading with PPIX.[19]

Table 3 – Effect of ENF and PPIX on the thermodynamic parameters of DMPC multilamellar vesicles membranes (average ± *SD*, *n*=2)

	T_{m1} (ºC)	ΔH_{m1} (kJ.mol^{-1})	T_{m2} (ºC)	ΔH_{m2} (kJ.mol^{-1})
DMPC	24.6 (±0.1)	29.1 (±2.0)	n.a.	n.a.
DMPC:ENF (50:1)	23.6 (±0.02)	2.7 (±2.0)	27.1 (±0.2)	14.1 (±1.0)
DMPC:ENF:PPIX (50:1:5)	23.8 (±0.3)	2.8 (±2.0)	26.3 (±0.7)	21.0 (±4.0)

n.a. – non-applicable

Combination of entry inhibitors within lipid bilayers of LUVs enhances synergistic activity

Anti-retroviral therapy regimens benefit from drug co-administration in single formulations. Such is evidenced by approved multi-class combination products, integrating up to three different antiretrovirals for single administration.[57] Previous studies have suggested that HIV-1 antiretrovirals combination in liposomal formulations is suitable for improved delivery of synergistic inhibitor classes towards $CD4^+$ T-cells.[58] Based on our previous observations, ENF and PPIX are potentially synergistic and compatible for simultaneous loading within LUVs membranes. We then compared the efficacy of single- and dual-loaded EI-LUV nanocarriers against HIV-1_{NL4-3} entry *in vitro*, using conventional and immune-evasive formulations (Fig. 4). Single entry inhibitor and ENF:PPIX (1:25) combination were pre-loaded into LUVs and simultaneously added with viruses to TZM-bl cells. To discard any background effects of LUVs on cell viability or HIV-1_{NL4-3} infectivity, we performed control experiments in the presence of LUVs (Fig. S3; Fig. S8). Single-loaded POPC LUVs had lower efficacy compared to the free entry inhibitors, while the opposite was observed for entry inhibitors loaded in POPC:DPPE-PEG_{2000} (9:1) LUVs (Table 1). In addition, dual-loaded EI-LUV were more potent than single-loaded ones, independently of the lipid composition, resulting in a characteristic dose-response curve shift. To further evaluate entry inhibitors synergy in dual-loaded EI-LUV systems we applied the comparative and quantitative approaches mentioned above (Fig. 5). The median-effects plots for dual-loaded EI-LUV composed of POPC overlapped with the Bliss Independence model, as previously observed for free entry inhibitors

combination (Fig. 5, A). POPC:DPPE-PEG$_{2000}$ EI-LUV showed higher efficacy than predicted by both the Loewe's Additivity and Bliss Independence models (Fig. 5, B). Deviation towards synergy from the Bliss prediction was observed at entry inhibitors concentrations above the IC_{50}. CI values were also lower for POPC:DPPE-PEG$_{2000}$ EI-LUV systems when compared to POPC EI-LUV and free entry inhibitors, suggesting remarkable improvement in synergy, especially at concentrations above the IC_{50} (Fig. 5, C). Values of CI for f_a < 0.5 should be discarded as error amplification due to poor noise/signal ratios make CI unreliable in this condition.[59]

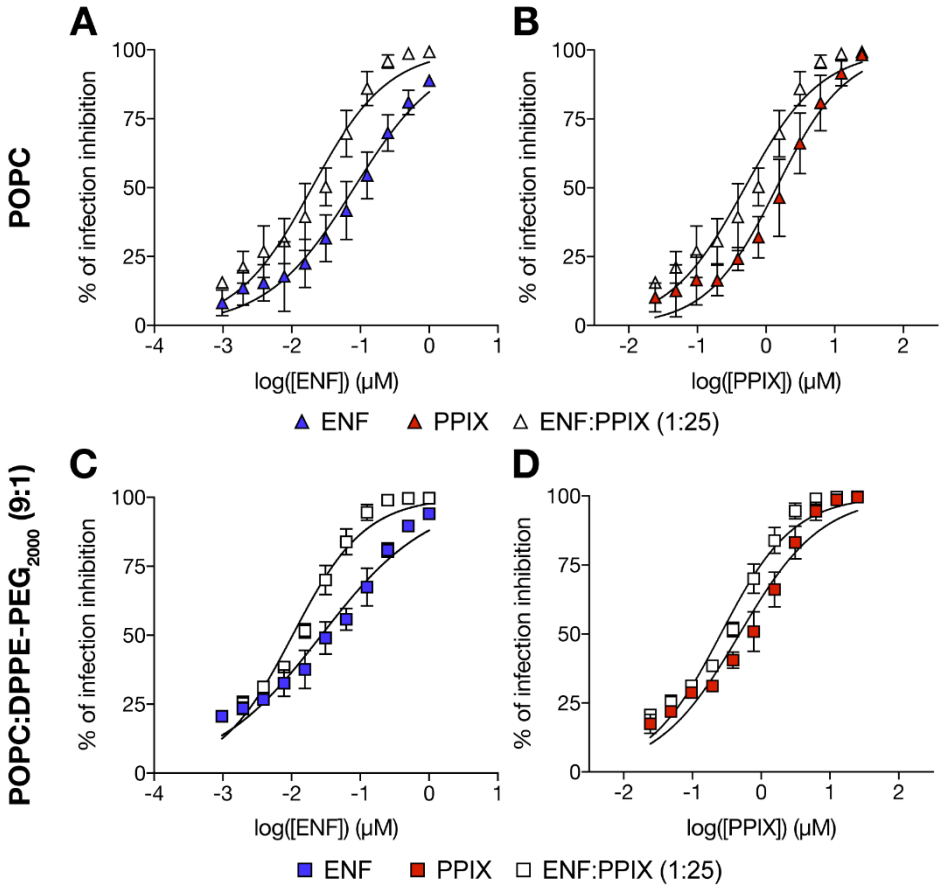

Figure 4 – Efficacy of single- and dual-loaded EI-LUV nanocarriers on HIV-1 entry *in vitro*. Dose-response curves of ENF, PPIX and ENF:PPIX (1:25) combination loaded within POPC (A and B) and POPC:DPPE-PEG$_{2000}$ (9:1) (C and D) LUVs membranes (500 μM) against HIV-1$_{NL4-3}$ entry into TZM-bl cells. Single- and dual-loaded EI-LUV were added simultaneously with HIV-1$_{NL4-3}$ (100 $TCID_{50}$) to TZM-bl cells. Viral infectivity was quantified 48 h post-infection through luciferase reporter-enzyme activity and converted to viral inhibition using Eq. 6 and 7. Results correspond to the average of three independent experiments.

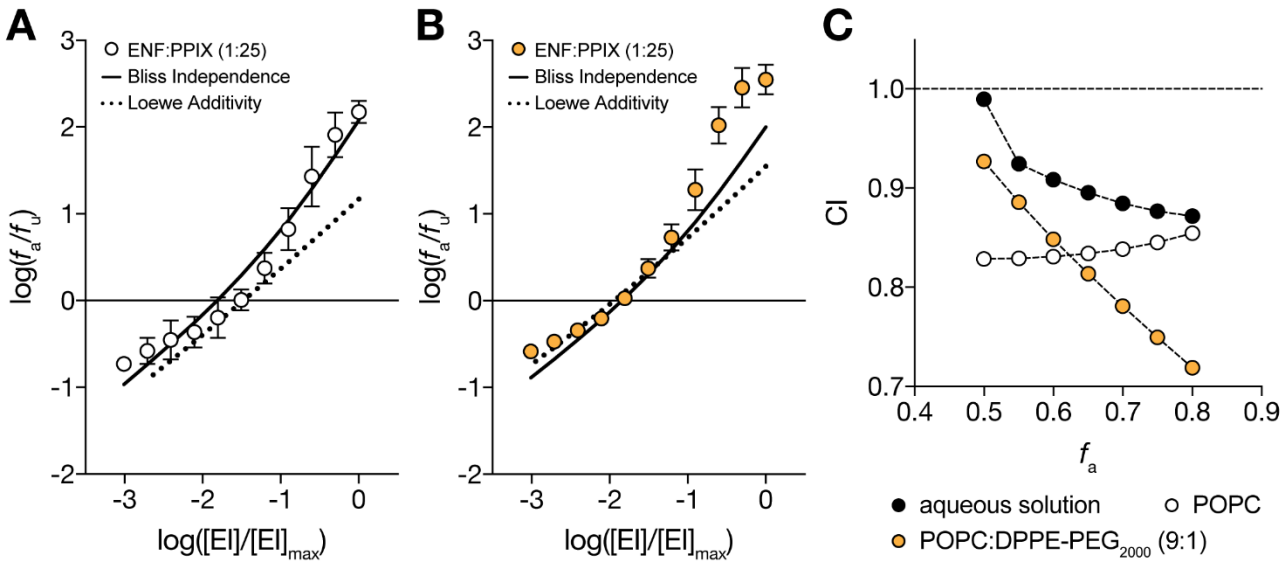

Figure 5 – Comparative and quantitative synergy analysis of ENF and PPIX combination in EI-LUV nanocarriers. (A and B) Median-effects plots of ENF:PPIX (1:25) combination loaded within POPC (A) and POPC:DPPE-PEG$_{2000}$ (9:1) (B) LUVs membranes against HIV-1$_{NL4-3}$ entry *in vitro*, compared to the predicted Bliss Independence and Loewe's Additivity models. Models predictions were determined through Eq. 9 and 10. Effects that exceeded the predicted models are considered as synergistic. Results correspond to the average of three independent replicates. **(C)** Chou-Talalay quantitative CI analysis of ENF:PPIX (1:25) combinations in aqueous solution and loaded within LUVs membranes. CI values were determined through Eq. 11. Combination CI values below the unit (dashed line) are evidence of synergy. Results correspond to one of three independent replications.

Since entry inhibitor act extracellularly and are incorporated within lipid membranes, one cannot exclude that slowed release and/or slowed cell-mediated clearance, hallmarks of PEG-coated liposomes, are on the basis of the observed improved dose reduction. An analogous improvement in synergy was reported for antiretroviral MVC-etravirine dual-loaded poly(lactic-co-glycolic acid) (PLGA) nanoparticles.[60] MVC-etravirine efficacy, moderately synergistic in aqueous solution, exceeded the predictions of the Bliss model when combined in nanoparticles. An independent study combining nevirapine and saquinavir antiretrovirals within PEG-coated eggPC:Chol:DSPE-PEG liposomes lumen, reported an improvement in efficacy compared to combination in the absence of liposomes.[58] Despite the lack of a more detailed synergy analysis in this case, the authors showed clear evidence of combination dose reduction through targeted delivery to CD4 expressing cells.

The mechanism behind the reported synergy and dose reduction enhancement provided by liposomes remains unclear. Other authors have suggested that this may correlate with drug formulations and intracellular trafficking mediated by the delivery vehicles,[60] which was also proposed for anticancer drug combinations in nanosized delivery systems.[61,62] Since HIV-1 entry inhibitors act at the extracellular level, such hypothesis is not valid to explain EI-LUV efficacy. Lower synergy with experimental data being described by the Bliss model suggests that ENF and PPIX act by independent and uncorrelated mechanisms in the absence of a LUV or in the presence

of POPC LUV. The key for synergy is associated to the carrier, which calls for revisiting the importance of nanocarrier transporters as synergy enhancers in combined therapies. It is plausible that cell membranes and viral proteins compete for entry inhibitors shifting its partition equilibrium towards release in extracellular sites relevant for the mode of action. PEG coatings, which prevent protein opsonization, may also contribute towards this end. Future studies using *in vivo* infection models are required to further characterize the role of liposomes in entry inhibitors synergy of clinical importance.

Conclusion

Entry inhibitors are underused despite their therapeutic potential due to suboptimal pharmacological properties. We have developed a liposome delivery system combining two clinically relevant entry inhibitors, ENF and PPIX, never tested before for synergy against HIV-1. This combination takes advantage of the complementary lipid interaction shared by the entry inhibitors to efficiently co-load both compounds in a single liposomal carrier. This approach has potential application to entry inhibitor lipopeptides (peptides conjugated to a hydrophobic moiety) which are highly lipophilic and can become tightly anchored to lipid membranes, exposing the entry inhibitor peptide domain through a flexible linker.[63-65] Our results show that immune-evasive POPC:DPPE-PEG_{2000} (9:1) LUVs (average D_H of 120 nm) are suitable alternatives to conventional liposomes, significantly enhancing entry inhibitors synergy compared to the combination in free aqueous form, bringing new hope to a refreshed more complete use of entry inhibitors in the clinics. Future studies will focus on evaluating the *in vivo* performance of the dual-loaded nanocarrier system compared to the entry inhibitors combination in free form, exploring the viability of intravenous and intramuscular administration routes.[18]

Materials and Methods

Chemicals and reagents

ENF and HIV-1_{NL4-3} molecular clone (*pNL4-3*) were provided by the NIH AIDS Research and Reference Reagent Program, Division of AIDS, NIAID, NIH (Bethesda, MD, USA). PPIX was purchased from Frontier Scientific (Logan, UT, USA) or Sigma-Aldrich (St. Louis, MO, USA). DEX (MW=8500 Da), 5-NS, 16-NS, and $CaCl_2$ were purchased from Sigma-Aldrich (St. Louis, MO, USA). N-2-hydroxyethylpiperazine-N′-2-ethanesulfonic acid (HEPES), NaCl, Na_2HPO_4, tris(hydroxymethyl)aminomethane hydrochloride (Tris-HCl), ethylenedinitrilotetraacetic acid (EDTA), dimethyl sulfoxide (DMSO), ethanol, and chloroform (the last three with spectroscopic grade) were purchased from Merck (Darmstadt, Germany). Dulbecco's Modified Eagle's Medium (DMEM), fetal bovine serum (FBS) and penicillin-streptomycin (Pen-Strep) were obtained from Gibco (Thermo-Fisher, Waltham, MA, USA). The Luc-Screen® luciferase detection system was obtained from Applied Biosystems (Thermo-Fisher). Lipids POPC, DPPE-PEG_{2000}, and DMPC were purchased from Avanti (Alabaster, AL, USA). AlamarBlue® reagent was purchased from Invitrogen (Thermo-Fisher).

Cells and virus culture

Human embryonic kidney 293T (HEK293T) and TZM-bl cell lines were purchased from ATCC (Manassas, VA, USA). Cells were cultured in DMEM supplemented with 10% (v/v) FBS and 100 U/mL Pen-Strep (complete medium), and incubated at 37 ºC, in a 5% CO_2 atmosphere. These conditions were applied to all cell culture incubation periods.

Recombinant HIV-1_{NL4-3} viruses were produced in HEK293T cell cultures transfected with the *pNL4-3* infectious clone through the calcium phosphate co-precipitation method.[66,67] HEK293T cells were seeded at $5x10^5$ cells/well in tissue culture-treated 6-well microplates from TPP (Trasadingen, Switzerland), and incubated for 24 h. To prepare calcium-phosphate-DNA transfection mixtures, *pNL4-3* DNA (3.5 µg/well) was initially diluted in 1 mM Tris-HCl, 0.1 mM EDTA, 250 mM $CaCl_2$, pH 7.6 and then added, drop by drop, to an equal volume of 50 mM HEPES, 280 mM NaCl, 1.5 mM Na_2HPO_4, pH 7.05, under gentle agitation. Transfection mixtures were allowed to incubate at room temperature, for 20 min, before addition to cells. After 18 h, transfection mixtures were replaced with fresh complete medium. Viral supernatants were collected 48 h post-transfection, centrifuged at 315 *g* for 5 min to remove cell debris, and stored at -80 ºC until used.

Viral supernatants harvested from *pNL4-3*-transfected HEK293T cells were titered through the Reed-Muench method,[68] based on HIV-1_{NL4-3} infectivity against TZM-bl cell cultures. TZM-bl cells were seeded at $2x10^4$ cells/well in tissue culture-treated 96-well microplates from Corning (Corning, NY, USA), and incubated for 24 h. Cells were then incubated with serial dilutions (2-fold) of viral supernatants for 3 h, after which the supernatant was replaced with fresh complete medium. After 45 h, TZM-bl cell infection was quantified through luciferase reporter-gene expression levels, under the control of an HIV-1 TAT-dependent LTR promoter,[69] using the Luc-Screen® luciferase chemiluminescence detection system. Luminescence was measured in an Infinite M200 microplate reader from Tecan (Männedorf, Switzerland). Cells were considered to be infected if the respective luminescence intensity, *L*, was 5-fold higher compared to the intensity from control cells, in the absence of viruses. Titration was performed with at least four replicates to allow accurate estimation of HIV_{NL4-3} 50% tissue culture infectious dose ($TCID_{50}$) of viral supernatants.

Entry inhibitors and liposomes samples preparation

Lyophilized ENF was dissolved in 10 mM HEPES, 150 mM NaCl, pH 7.4 (sample buffer) to final concentrations of 1 mg/mL, sonicated in an ultrasonic bath for 10 min, and stored at -20 ºC. PPIX was dissolved in 100% DMSO to final concentrations of 1 mg/mL, and stored at -20 ºC. ENF and PPIX stock solutions were diluted to final working concentrations in sample buffer for biophysical experiments and in complete media for *in vitro* HIV-1_{NL4-3} inhibition experiments. DMSO content was kept below 0.5% (v/v) in the presence of cells to prevent cell death and below 2% (v/v) in all other experiments.

Liposome suspensions were prepared as described elsewhere.[70] Lipid formulations were first dissolved with chloroform in a round-bottom flask. Then, a thin film was formed by solvent evaporation and lipid drying under a stream of nitrogen and then in vacuum, overnight. Rehydration with sample buffer and a series of 8-10 freeze/thaw cycles yielded a multilamellar vesicles suspension. LUVs with the desired diameter were obtained

from extrusion of the multilamellar vesicles through a 100 nm pore Nucleopore polycarbonate membrane purchased from Whatman/GE Healthcare (Kent, United Kingdom). Extrusion was performed in a LiposoFast-Basic plus Stabilizer setup from Avestin (Mannheim, Germany). POPC, DMPC, and POPC:DPPE-PEG_{2000} (9:1) liposome formulations were prepared.

Fluorescence spectroscopy studies

Fluorescence spectroscopy measurements were carried out in a FLS920 spectrofluorometer from Edinburgh Instruments (Livingston, UK). All measurements were performed at 25 ºC.

Lipid membrane partition experiments were performed by successive additions of LUVs (15 mM) aliquots to ENF or PPIX solutions (10 μM), covering final lipid concentrations between 0 and 5 mM. A 10 min incubation period was allowed between each lipid addition. The extent of partition to lipid membranes was followed by entry inhibitors steady-state fluorescence emission intensity, measured at each lipid concentration. Excitation wavelengths (λ_{exc}) used were 280 nm for ENF Trp and 397 nm for PPIX. Excitation slits were 3 and 1 nm for ENF and PPIX, respectively. Emission slits were 10 nm. Fluorescence intensity was corrected for dilution, background and light scattering.[71] K_p values were determined from non-linear regression fit of equation 1 to experimental data:[43,72]

$$\frac{I}{I_W} = \frac{1 + K_p \gamma_L \frac{I_L}{I_W}[L]}{K_p \gamma_L [L]} \quad (1)$$

in which I_W and I_L are the integrated fluorescence emission intensities in aqueous solution and in lipid, respectively, γ_L is the lipid molar volume and [L] the lipid concentration. The kinetics of entry inhibitor partition towards lipid membranes were assessed through a time-resolved fluorescence approach. PPIX and ENF (10 μM) fluorescence emission intensity was monitored for 1 min prior to the addition of POPC and POPC:DPPE-PEG_{2000} (9:1) LUVs (5 mM), and for 10 minutes afterwards. Emission wavelengths (λ_{emi}) were fixed at 335 nm for ENF Trp and 635 nm for PPIX. Intensity values were corrected for background and dilution.

Entry inhibitors intra-membrane depth determination experiments were performed by successive additions of either 5-NS or 16-NS lipophilic quenchers dissolved in ethanol to ENF or PPIX (10 μM) samples in the presence of LUVs (3 mM). Ethanol content was kept below 2% (v/v). A 10 min incubation period was allowed between each addition. The extent of fluorescence quenching by 5-NS and 16-NS, which correlates with the extent of membrane penetration, was followed by entry inhibitors steady-state fluorescence emission intensity, measured for each quencher concentration using the same experimental conditions as described for partition experiments. Quenching data was analyzed through linear regression with the Stern-Volmer relationship:[73]

$$\frac{I_0}{I} = 1 + K_{SV}[Q]_L \quad (2)$$

in which, I_0 and I correspond to the integrated fluorescence emission intensities in the absence and presence of quencher, respectively, K_{SV} is the Stern-Volmer constant and $[Q]_L$ is the effective molar concentration of quencher in the LUV membrane itself. $[Q]_L$ was calculated from the K_p values of both quenchers towards fluid-

phase lipid bilayers.[72] Intra-membrane fluorophore depth localization profiles were estimated as described elsewhere.[74]

Entry inhibitors co-localization in LUVs membranes (dual-loading) was assessed by FRET between ENF Trp (donor) and PPIX (acceptor). ENF and PPIX (10 μM) were co-incubated in sample buffer or in the presence of LUVs (200 μM) for 10 min, before performing measurements. ENF Trp fluorescence emission spectra were collected from 300 to 450 nm, using a λ_{exc} of 280 nm. Excitation and emission slits were 3 and 10 nm, respectively. Fluorescence intensity was corrected for donor-acceptor shared excitation light.[75] The FRET efficiency between ENF and PPIX was quantified based on the following formalism:[73]

$$E = 1 - \frac{I_{\text{D-A}}}{I_{\text{D}}} \tag{3}$$

in which $I_{\text{D-A}}$ and I_{D} correspond to the donor integrated fluorescence emission intensities in the presence and absence of acceptor, respectively.

Dynamic light scattering

DLS experiments were carried out on a Zetasizer Nano ZS from Malvern (Worcestershire, UK) using polystyrene folded capillary cells (DTS1070). All measurements were performed at 25 ºC.

LUVs (500 μM) were pre-incubated with increasing concentrations of ENF, PPIX and ENF:PPIX (1:25) combination for 15 min, at 25 ºC, before initiating measurements. Entry inhibitors concentrations ranged from 0 to 25 μM for PPIX and 0 to 1 μM for ENF. LUVs average D_H and PDI were measured using DLS in particle size analysis mode. Measurements consisted in a set of 10 individual runs (~16 scans), each corresponding to a scattered intensity autocorrelation function. Normalized autocorrelation functions were analyzed using the cumulants[76] and CONTIN[77,78] methods, yielding the distribution of diffusion coefficients (D) in the sample. This parameter was used for the calculation of the distribution-averaged D_H through the Stokes-Einstein-Sutherland relationship:[79,80]

$$D = \frac{k_{\text{b}} T}{3\pi\eta D_H} \tag{4}$$

where, k_{b} is the Boltzmann constant, T the absolute temperature, and η the medium viscosity. The average D_H is mathematically equivalent to the Z-average. PDI values were calculated through the relationship PDI = $(D_H)^2/(SD)^2$, in which the SD is the respective standard deviation.

LUVs surface charge density was measured using DLS in ζ-potential analysis mode (laser Doppler electrophoresis). Samples were prepared as described for DLS particle size analysis. Measurements consisted in a set of 10 individual runs (~100 scans), each corresponding to a value of electrophoretic mobility (μ_e) determined through phase analysis light scattering (PALS). Experiments were performed under a constant applied voltage of 30 V. ζ-potential values were calculated through Henry's equation:[81,82]

$$\mu_e = \frac{2\varepsilon_r \varepsilon_0 \zeta \, F(\kappa a)}{3\eta} \tag{5}$$

where ε_r is the relative permittivity/dielectric constant, ε_0 is the permittivity of vacuum, F(κa) is the Henry function and η is the medium viscosity at the experimental temperature. The value of F(κa) was assumed to be 1.5 for aqueous media.

Differential scanning calorimetry

DSC experiments were performed on a NanoDSC calorimeter from TA Instruments (New Castle, DE, USA). ENF (1 mM stock solution in PBS) was added to a suspension of DMPC multilamellar vesicles (1 mg/mL lipid concentration; 1.47 mM) in PBS to peptide/lipid molar ratios of 1/50. In the case of ENF and PPIX combination, ENF (1 mM stock solution in PBS) and PPIX (17.8 mM stock solution in DMSO) were added to the multilamellar vesicles suspension to reach entry inhibitor/lipid ratio of 1/50 and 1/10, respectively, in order to saturate the membranes with EI without compromising their integrity. Samples were scanned at 1°C/min between 0°C and 50°C at least 3 series of alternated heating and cooling scans. Analysis and deconvolution were performed using the NanoAnalyze software (TA Instruments), using a two-state model.

In vitro inhibition of HIV-1_{NL4-3} infection

The inhibitory activity of ENF, PPIX and ENF:PPIX (1:25) combination (with and without LUVs) on HIV-1_{NL4-3} entry into TZM-bl cells was evaluated as previously described.[83] TZM-bl cells were seeded at $2x10^4$ cells/well in tissue culture-treated 96-well microplates and incubated for 24 h. Cells were then incubated with serial dilutions (2-fold) of either single entry inhibitor or combination and, simultaneously, with HIV-1_{NL4-3} viral supernatants (100 $TCID_{50}$/well) for 3 h, after which the infection mixture was replaced with fresh complete medium. ENF, PPIX and ENF:PPIX (1:25) combination were allowed to pre-incubate with LUVs (500 μM) for 10 min, to allow efficient entry inhibitors loading into lipid membranes. For the time-of-inhibitor-addition experiments, entry inhibitor serial dilutions were instead added to cells at -1 h, +1 h, +2 h or +3 h relatively to the moment of infection with HIV-1_{NL4-3} viral supernatants. Untreated cells (in the absence of entry inhibitors) were used as a control. After 45 h, TZM-bl cells infection was quantified through luciferase reporter-gene expression levels using the Luc-Screen® chemiluminescence detection system. Luminescence, *L*, measurements were performed in an Infinite M200 microplate reader. *L* values were analyzed through non-linear regression with the classical dose-response relationship (median-effects model based on mass action):[84]

$$f_a = \frac{1}{1+\left(\frac{IC_{50}}{[EI]}\right)^m} \quad (6)$$

$$f_a = 1 - \frac{L}{L_0} \quad (7)$$

where, f_a is the fraction of inhibited virues, IC_{50} is the entry inhibitor concentration at 50% inhibition, *m* is a slope parameter mathematically analogous to the Hill slope, [EI] is the entry inhibitor concentration, and L_0 is the luminescence intensity of infected cell cultures in the absence of entry inhibitors. For clarity, dose-response curves were represented as percentage of inhibition vs log([EI]).

Cytotoxicity studies

The cytotoxic effects of each entry inhibitor, respective combination and loaded LUVs on TZM-bl cell cultures were assessed using a resazurin reduction fluorometric assay. Resazurin, the active compound in alamarBlue®, is a blue dye that can be reduced to a pink fluorescent intermediate, resorufin, as a result of cell metabolic activity.[85] TZM-bl cells were seeded at $2x10^4$ cells/well in tissue culture-treated 96-well microplates and incubated for 24 h. Cells were then incubated with serial dilutions (2-fold) of single entry inhibitor or combination, with and without addition of LUVs, for 3 h, after which the mixture was replaced with fresh complete medium. Untreated cells (in the absence of entry inhibitors) were used as a control. After 42 h, media was replaced with alamarBlue® reagent and incubated for an additional 3 h. Resazurin reduction was quantified by resorufin fluorescent emission intensity, measured in an Infinite M200 microplate reader. Fluorescence emission intensity was collected at 590 nm, using a fixed λ_{exc} of 560 nm. Excitation and emission slits were 9 and 20 nm, respectively. Cell viability was calculated through the following formalism:

$$\% \text{ of viable cells} = \frac{I_{EI} - I_{background}}{I_{control} - I_{background}} \times 100\% \quad (8)$$

where I_{EI} corresponds to the resorufin fluorescence emission intensity in the presence of single entry inhibitors or combination, $I_{control}$ to the fluorescence emission intensity in the absence of entry inhibitors and $I_{background}$ to the background fluorescence emission from the non-reduced alamarBlue® reagent.

Synergy activity analysis

To characterize and quantify the extent of synergy on the activity of the ENF:PPIX (1:25) combination, a comparison of experimental data with theoretical expectations from reference additivity models was performed. For comparative analysis, dose-response data for single entry inhibitors and combination were plotted as median-effects $\log(f_a/f_u)$ vs $\log([EI]/[EI]_{max})$ graphs, in which f_a and f_u are the fraction of viruses affected and unaffected by the entry inhibitors, respectively, and $[EI]/[EI]_{max}$ is the concentration of entry inhibitor normalized to the maximum concentration used. Loewe Additivity[86] and Bliss Independence[87] models (with variable slope) expectations were calculated using equations 9 and 10, respectively:[31]

$$1 = \frac{[EI]_1}{IC_{50_1}\left(\frac{f_{a1+2}}{f_{u1+2}}\right)^{1/m_1}} + \frac{[EI]_2}{IC_{50_2}\left(\frac{f_{a1+2}}{f_{u1+2}}\right)^{1/m_2}} \quad (9)$$

$$f_{u1+2} = \frac{1}{1+\left(\frac{[EI]_1}{IC_{50_1}}\right)^{m_1}} \times \frac{1}{1+\left(\frac{[EI]_2}{IC_{50_2}}\right)^{m_2}} \quad (10)$$

IC_{50} and m correspond to the entry inhibitor concentration at 50% effect and slope parameter, respectively. Subscripts 1 and 2 refer to each entry inhibitor separately and 1+2 to the combination of both. A detailed description of mathematical development of each model and their physical meaning in molecular terms is provided in section 1 of the supporting information. These models serve to set thresholds that separate synergy

from antagonism based on their individual performances. The Loewe Additivity model assumes that two inhibitors, acting independently, without interfering with each other, will have separate effects which add to produce the final effect, while the Bliss model is probabilistic: if drugs are independent from each other, then the probability of finding unaffected targets in the mixture is the product of finding unaffected targets when using each of the inhibitors alone. Entry inhibitors combination antiretroviral efficacy was considered to be synergistic if the experimental $\log(f_a/f_u)$ was higher than the effect predicted by at least one of the models.[31]

In addition to the models above, for direct quantitative analysis, the CI was calculated for the entry inhibitors combination according to the Chou-Talalay method:[88]

$$CI = \frac{[EI]_1'}{[EI]_1} + \frac{[EI]_2'}{[EI]_2} \quad (11)$$

in which $[EI]_i$ and $[EI]_i$' correspond to the concentrations of entry inhibitors$_i$ (i=1 or 2) alone or in combination, respectively, capable of inducing the same inhibitory effect. CI values were determined for the 50 to 80 % inhibition range, since synergy at high effect levels is more therapeutically relevant for infectious diseases.[59] CI>1 indicates antagonism, CI=1 indicates additivity and CI<1 indicates synergy.

Statistical analysis

Linear and non-linear regression analysis with the aforementioned equations was performed using GraphPad Prism®. Error bars on presented data represent the standard deviation (SD).

Associated Content

Supporting Information

Supporting Information is available free of charge from the ACS Publications website (http://pubs.acs.org/journal/ancac3).

Description of the reference additivity mathematical models for synergy predictions (Fig. S1), time-of-inhibitor-addition efficacy studies (Fig. S2), entry inhibitor cytotoxicity (Fig. S3), synergy analysis (Fig. S4), time-resolved fluorescence emission (Fig. S5) fluorescence emission quenching (Fig. S6), EI-LUV nanocarrier colloidal stability (Fig. S7) and viral infectivity controls (Fig. S8).

Financial interest statement

The authors declare no competing financial interest.

Author Information

Corresponding authors

*Correspondence to: Ana Salomé Veiga, Instituto de Medicina Molecular, Faculdade de Medicina, Universidade de Lisboa, Av. Prof. Egas Moniz, 1649-028 Lisboa, Portugal. E-mail: aveiga@medicina.ulisboa.pt

Astrid Walrant, Sorbonne Université, École normale supérieure, PSL University, CNRS, Laboratoire des Biomolécules, LBM, 4 Place Jussieu, 75005 Paris, France. E-mail: astrid.walrant@upmc.fr

Acknowledgements

This work was supported by European Research Area Networks (ERA-Net) project HIVERA/0002/2013 and Fundação para a Ciência e a Tecnologia (FCT-MCTES) project VIH/SAU/0029/2011. T.N.F., M.M.D. and I.C. acknowledge individual fellowships SFRH/BD/5283/2013, SFRH/BPD/122779/2016 and SFRH/BPD/65531/2009 funded by FCT-MCTES, respectively. A.S.V. acknowledges funding under the Investigator Programme (IF/00803/2012) from FCT-MCTES.

Abreviations

5-NS, 5-doxyl stearic acid; 16-NS, 16-doxyl stearic acid; CI, combination index; D_H, hydrodynamic diameter; DEX, dextran sulfate; DSC, differential scanning calorimetry; DLS, dynamic light scattering; DMEM, Dulbecco's Modified Eagle's Medium; DMPC, 1,2-dimyristoyl-*sn*-glycero-3-phosphocholine; DMSO, dimethyl sulfoxide; DPPE-PEG_{2000}, 1,2-dipalmitoyl-*sn*-glycero-3-phosphoethanolamine-*N*-[methoxy(polyethylene glycol)-2000]; ENF, enfuvirtide; HEK293T, human embryonic kidney 293T cell line; Env, HIV-1 viral envelope glycoproteins; FBS, fetal bovine serum; FRET, Förster Resonance Energy Transfer; HIV-1, human immunodeficiency virus type 1; LUV, large unilamellar vesicle; MVC, maraviroc; PALS, phase analysis light scattering; PBS, phosphate buffered saline; PDI, polydispersity index; Pen-Strep, penicillin-streptomycin; PLGA, poly(lactic-co-glycolic acid); POPC, 1-palmitoyl-2-oleoyl-*sn*-glycero-3-phosphocholine; PPIX, protoporphyrin IX; $TCID_{50}$, 50% tissue culture infectious dose;

References

(1) Blumenthal, R.; Durell, S.; Viard, M. HIV entry and envelope glycoprotein-mediated fusion. *JBC* **2012**, *287* (49), 40841–40849 DOI: 10.1074/jbc.R112.406272.

(2) Pancera, M.; Zhou, T.; Druz, A.; Georgiev, I. S.; Soto, C.; Gorman, J.; Huang, J.; Acharya, P.; Chuang, G.-Y.; Ofek, G.; et al. Structure and immune recognition of trimeric pre-fusion HIV-1 Env. *Nature* **2014**, *514* (7523), 455–461 DOI: 10.1038/nature13808.

(3) Melikyan, G. B. Membrane Fusion Mediated by Human Immunodeficiency Virus Envelope Glycoprotein. In *Membrane Fusion Mediated by Human Immunodeficiency Virus Envelope Glycoprotein*; Current Topics in Membranes; Elsevier, 2011; Vol. 68, pp 81–106.

(4) Haqqani, A. A.; Tilton, J. C. Entry inhibitors and their use in the treatment of HIV-1 infection. *Antiviral Res* **2013**, *98* (2), 158–170 DOI: 10.1016/j.antiviral.2013.03.017.

(5) Ugolini, S.; Mondor, I.; Parren, P. W. H. I.; Burton, D. R.; Tilley, S. A.; Klasse, P. J.; Sattentau, Q. J. Inhibition of Virus Attachment to CD4+ Target Cells Is a Major Mechanism of T Cell Line–adapted HIV-1 Neutralization. *Journal of Experimental Medicine* **1997**, *186* (8), 1287–1298 DOI: 10.1084/jem.186.8.1287.

(6) Shaheen, F.; Collman, R. G. Co-receptor antagonists as Hiv-1 entry inhibitors. *Current Opinion in Infectious Diseases* **2004**, *17* (1), 7–16 DOI: 10.1097/00001432-200402000-00003.

(7) Qadir, M. I.; Malik, S. A. HIV fusion inhibitors. *Rev Med Virol* **2010**, *20* (1), 23–33 DOI: 10.1002/rmv.631.

(8) Berkhout, B.; Eggink, D.; Sanders, R. W. Is there a future for antiviral fusion inhibitors? *Curr Opin Virol* **2012**, *2* (1), 50–59 DOI: 10.1016/j.coviro.2012.01.002.

(9) Henrich, T. J.; Kuritzkes, D. R. HIV-1 entry inhibitors: recent development and clinical use. *Curr Opin Virol* **2013**, *3* (1), 51–57 DOI: 10.1016/j.coviro.2012.12.002.

(10) Martin-Carbonero, L. Discontinuation of the clinical development of fusion inhibitor T-1249. *AIDS reviews*. January 2004, p 61.

(11) Nichols, W. G.; Steel, H. M.; Bonny, T.; Adkison, K.; Curtis, L.; Millard, J.; Kabeya, K.; Clumeck, N. Hepatotoxicity observed in clinical trials of aplaviroc (GW873140). *Antimicrobial Agents and Chemotherapy* **2008**, *52* (3), 858–865 DOI: 10.1128/AAC.00821-07.

(12) Hanna, G. J.; Lalezari, J.; Hellinger, J. A.; Wohl, D. A.; Nettles, R.; Persson, A.; Krystal, M.; Lin, P.; Colonno, R.; Grasela, D. M. Antiviral activity, pharmacokinetics, and safety of BMS-488043, a novel oral small-molecule HIV-1 attachment inhibitor, in HIV-1-infected subjects. *Antimicrobial Agents and Chemotherapy* **2011**, *55* (2), 722–728 DOI: 10.1128/AAC.00759-10.

(13) Chopra, S.; Venkatesan, N.; Betageri, G. V. Liposomes as nanocarriers for anti-HIV therapy. *Drug Deliv Trans Res* **2013**, *3* (5), 471–478 DOI: 10.1007/s13346-013-0134-2.

(14) Franquelim, H. G.; De-Sousa, F. F.; Veiga, A. S.; Santos, N. C.; Castanho, M. A. Cationic liposomes are possible drug-delivery systems for HIV fusion inhibitor sifuvirtide. *Soft Matter* **2011**, *7* (23), 11089–11092 DOI: 10.1039/c1sm06553j.

(15) Immordino, M. L.; Dosio, F.; Cattel, L. Stealth liposomes: review of the basic science, rationale, and clinical applications, existing and potential. *Int J Nanomedicine* **2006**, *1* (3), 297–315.

(16) Sercombe, L.; Veerati, T.; Moheimani, F.; Wu, S. Y.; Sood, A. K.; Hua, S. Advances and Challenges of Liposome Assisted Drug Delivery. *Front. Pharmacol.* **2015**, *6* (127), 215 DOI: 10.1038/sj.clpt.6100400.

(17) Kraft, J. C.; Freeling, J. P.; Wang, Z.; Ho, R. J. Y. Emerging research and clinical development trends of liposome and lipid nanoparticle drug delivery systems. *J Pharm Sci* **2014**, *103* (1), 29–52 DOI: 10.1002/jps.23773.

(18) Bulbake, U.; Doppalapudi, S.; Kommineni, N.; Khan, W. Liposomal Formulations in Clinical Use: An Updated Review. *Pharmaceutics* **2017**, *9* (2) DOI: 10.3390/pharmaceutics9020012.

(19) Veiga, S.; Henriques, S.; Santos, N. C.; Castanho, M. Putative role of membranes in the HIV fusion inhibitor enfuvirtide mode of action at the molecular level. *Biochem J* **2004**, *377* (Pt 1), 107–110 DOI: 10.1042/BJ20031350.

(20) Veiga, A. S.; Santos, N. C.; Loura, L. M. S.; Fedorov, A.; Castanho, M. A. R. B. HIV fusion inhibitor peptide T-1249 is able to insert or adsorb to lipidic bilayers. Putative correlation with improved efficiency. *JACS* **2004**, *126* (45), 14758–14763 DOI: 10.1021/ja0459882.

(21) Franquelim, H. G.; Loura, L. M. S.; Santos, N. C.; Castanho, M. A. R. B. Sifuvirtide screens rigid membrane surfaces. establishment of a correlation between efficacy and membrane domain selectivity among HIV fusion inhibitor peptides. *JACS* **2008**, *130* (19), 6215–6223 DOI: 10.1021/ja711247n.

(22) Badani, H.; Garry, R. F.; Wimley, W. C. Peptide entry inhibitors of enveloped viruses: The importance of interfacial hydrophobicity. *BBA* **2014**, *1838*, 2180–2197 DOI: 10.1016/j.bbamem.2014.04.015.

(23) Matthews, T.; Salgo, M.; Greenberg, M.; Chung, J.; DeMasi, R.; Bolognesi, D. Enfuvirtide: the first therapy to inhibit the entry of HIV-1 into host CD4 lymphocytes. *Nat Rev Drug Disc* **2004**, *3* (3), 215–225 DOI: 10.1038/nrd1331.

(24) Cruz-Oliveira, C.; Almeida, A. F.; Freire, J. M.; Caruso, M. B.; Morando, M. A.; Ferreira, V. N. S.; Assunção-Miranda, I.; Gomes, A. M. O.; Castanho, M. A. R. B.; Da Poian, A. T. Mechanisms of Vesicular Stomatitis Virus Inactivation by Protoporphyrin IX, Zinc-Protoporphyrin IX, and Mesoporphyrin IX. *Antimicrobial Agents and Chemotherapy* **2017**, *61* (6), e00053–17 DOI: 10.1128/AAC.00053-17.

(25) Adler-Moore, J. P.; Proffitt, R. T. Development, characterization, efficacy and mode of action of ambisome, a unilamellar liposomal formulation of amphotericin b. *J Liposome Res* **1993**, *3* (3), 429–450 DOI: 10.3109/08982109309150729.

(26) Van Etten, E.; Snijders, S. V.; Van Vianen, W.; Bakker-Woudenberg, I. Superior efficacy of liposomal amphotericin B with prolonged circulation in blood in the treatment of severe candidiasis in leukopenic mice. *Antimicrobial Agents and Chemotherapy* **1998**, *42* (9), 2431–2433.

(27) Moribe, K.; Maruyama, K.; Iwatsuru, M. Molecular localization and state of amphotericin B in PEG liposomes. *Int J Pharm* **1999**, *193* (1), 97–106 DOI: 10.1016/S0378-5173(99)00323-3.

(28) Joly, V.; Jidar, K.; Tatay, M.; Yeni, P. Enfuvirtide: from basic investigations to current clinical use. *Expert Opin Pharmacother* **2010**, *11* (16), 2701–2713 DOI: 10.1517/14656566.2010.522178.

(29) Sachar, M.; Anderson, K. E.; Ma, X. Protoporphyrin IX: The good, the bad, and the ugly. *J. Pharmacol. Exp. Ther.* **2016**, *356* (2), 267–275 DOI: 10.1124/jpet.115.228130.

(30) Seden, K.; Back, D.; Khoo, S. Antiretroviral drug interactions: often unrecognized, frequently unavoidable, sometimes unmanageable. *J Antimicrob Chemother* **2009**, *64* (1), 5–8 DOI: 10.1093/jac/dkp152.

(31) Jilek, B. L.; Zarr, M.; Sampah, M. E.; Rabi, S. A.; Bullen, C. K.; Lai, J.; Shen, L.; Siliciano, R. F. A quantitative basis for antiretroviral therapy for HIV-1 infection. *Nat. Med.* **2012**, *18* (3), 446–451 DOI: 10.1038/nm.2649.

(32) Neurath, A. R.; Strick, N.; Haberfield, P. Rapid prescreening for antiviral agents against HIV-1 based on their inhibitory activity in site-directed immunoassays. II. Porphyrins reacting with the V3 loop of gp120. *Antiviral Chemistry and Chemotherapy* **1992**, *3* (1), 55–63.

(33) Neurath, A. R.; Strick, N.; Lin, K.; Debnath, A. K.; Jiang, S. Tin protoporphyrin IX used in control of heme metabolism in humans effectively inhibits HIV-1 infection. *Antiviral Chemistry and Chemotherapy* **1994**, *5* (5), 322–330.

(34) Vzorov, A. N.; Dixon, D. W.; Trommel, J. S.; Marzilli, L. G.; Compans, R. W. Inactivation of Human Immunodeficiency Virus Type 1 by Porphyrins. *Antimicrobial Agents and Chemotherapy* **2002**, *46* (12), 3917–3925 DOI: 10.1128/AAC.46.12.3917-3925.2002.

(35) Assunção-Miranda, I.; Cruz-Oliveira, C.; Neris, R. L. S.; Figueiredo, C. M.; Pereira, L. P. S.; Rodrigues, D.; Araujo, D. F. F.; Da Poian, A. T.; Bozza, M. T. Inactivation of Dengue and Yellow Fever viruses by heme, cobalt-protoporphyrin IX and tin-protoporphyrin IX. *Proceedings of the Society of Agricultural Bacteriologists* **2016**, *120* (3), 790–804 DOI: 10.1111/jam.13038.

(36) Tremblay, C. L.; Kollmann, C.; Giguel, F.; Chou, T. C.; Hirsch, M. S. Strong in vitro synergy between the fusion inhibitor T-20 and the CXCR4 blocker AMD-3100. *J. Acquir. Immune Defic. Syndr.* **2000**, *25* (2), 99–102.

(37) Nagashima, K. A.; Thompson, D. A.; Rosenfield, S. I.; Maddon, P. J.; Dragic, T.; Olson, W. C. Human immunodeficiency virus type 1 entry inhibitors PRO 542 and T-20 are potently synergistic in blocking virus-cell and cell-cell fusion. *J. Infect. Dis.* **2001**, *183* (7), 1121–1125 DOI: 10.1086/319284.

(38) Roell, K. R.; Reif, D. M.; Motsinger-Reif, A. A. An Introduction to Terminology and Methodology of Chemical Synergy-Perspectives from Across Disciplines. *Front. Pharmacol.* **2017**, *8*, 158 DOI: 10.3389/fphar.2017.00158.

(39) Dorr, P.; Westby, M.; Dobbs, S.; Griffin, P.; Irvine, B.; Macartney, M.; Mori, J.; Rickett, G.; Smith-Burchnell, C.; Napier, C.; et al. Maraviroc (UK-427,857), a potent, orally bioavailable, and selective small-molecule inhibitor of chemokine receptor CCR5 with broad-spectrum anti-human

immunodeficiency virus type 1 activity. *Antimicrobial Agents and Chemotherapy* **2005**, *49* (11), 4721–4732 DOI: 10.1128/AAC.49.11.4721-4732.2005.

(40) Cashen, A. F.; Nervi, B.; DiPersio, J. AMD3100: CXCR4 antagonist and rapid stem cell-mobilizing agent. *Future Oncol* **2007**, *3* (1), 19–27 DOI: 10.2217/14796694.3.1.19.

(41) Vail, D. M.; Macewen, E. G.; Kurzman, I. D.; Dubielzig, R. R.; Helfand, S. C.; Kisseberth, W. C.; London, C. A.; Obradovich, J. E.; Madewell, B. R.; Rodriguez, C. O.; et al. Liposome-Encapsulated Muramyl Tripeptide Phosphatidylethanolamine Adjuvant Immunotherapy for Splenic Hemangiosarcoma in the Dog: A Randomized Multi-Institutional Clinical Trial. *Clin. Cancer Res.* **1995**, *1* (10), 1165–1170.

(42) Dzieciuch, M.; Rissanen, S.; Szydłowska, N.; Bunker, A.; Kumorek, M.; Jamróz, D.; Vattulainen, I.; Nowakowska, M.; Róg, T.; Kępczyński, M. PEGylated Liposomes as Carriers of Hydrophobic Porphyrins. *J Phys Chem B* **2015**, *119* (22), 6646–6657 DOI: 10.1021/acs.jpcb.5b01351.

(43) Santos, N. C.; Prieto, M.; Castanho, M. A. R. B. Quantifying molecular partition into model systems of biomembranes: an emphasis on optical spectroscopic methods. *BBA* **2003**, *1612* (2), 123–135 DOI: 10.1016/S0005-2736(03)00112-3.

(44) Figueira, T. N.; Freire, J. M.; Cunha-Santos, C.; Heras, M.; Goncalves, J.; Moscona, A.; Porotto, M.; Salomé Veiga, A.; Castanho, M. A. R. B. Quantitative analysis of molecular partition towards lipid membranes using surface plasmon resonance. *Sci Rep* **2017**, *7*, 45647 DOI: 10.1038/srep45647.

(45) Hollmann, A.; Matos, P. M.; Augusto, M. T.; Castanho, M. A. R. B.; Santos, N. C. Conjugation of Cholesterol to HIV-1 Fusion Inhibitor C34 Increases Peptide-Membrane Interactions Potentiating Its Action. *PLoS ONE* **2013**, *8* (4), e60302 DOI: 10.1371/journal.pone.0060302.t003.

(46) Freire, J. M.; Veiga, A. S.; Rego de Figueiredo, I.; la Torre, de, B. G.; Santos, N. C.; Andreu, D.; Da Poian, A. T.; Castanho, M. A. R. B. Nucleic acid delivery by cell penetrating peptides derived from dengue virus capsid protein: design and mechanism of action. *FEBS J* **2014**, *281* (1), 191–215 DOI: 10.1111/febs.12587.

(47) Brown, S. B.; Shillcock, M.; Jones, P. Equilibrium and kinetic studies of the aggregation of porphyrins in aqueous solution. *Biochem J* **1976**, *153* (2), 279–285.

(48) Ulrich, A. S. Biophysical aspects of using liposomes as delivery vehicles. *Biosci Rep* **2002**, *22* (2), 129–150.

(49) Kraft, J. C.; Freeling, J. P.; Wang, Z.; Ho, R. J. Y. Emerging research and clinical development trends of liposome and lipid nanoparticle drug delivery systems. *J Pharm Sci* **2014**, *103* (1), 29–52 DOI: 10.1002/jps.23773.

(50) Nir, S.; Nieva, J. L. Interactions of peptides with liposomes: pore formation and fusion. *Prog. Lipid Res.* **2000**, *39* (2), 181–206.

(51) Carter, K. A.; Shao, S.; Hoopes, M. I.; Luo, D.; Ahsan, B.; Grigoryants, V. M.; Song, W.; Huang, H.; Zhang, G.; Pandey, R. K.; et al. Porphyrin-phospholipid liposomes permeabilized by near-infrared light. *Nat Commun* **2014**, *5*, 3546 DOI: 10.1038/ncomms4546.

(52) Khurshid, S.; Saridakis, E.; Govada, L.; Chayen, N. E. Porous nucleating agents for protein crystallization. *Nat Protoc* **2014**, *9* (7), 1621–1633 DOI: 10.1038/nprot.2014.109.

(53) Narenji, M.; Talaee, M. R.; Moghimi, H. R. Investigating the effects of size, charge, viscosity and bilayer flexibility on liposomal delivery under convective flow. *Int J Pharm* **2016**, *513* (1-2), 88–96 DOI: 10.1016/j.ijpharm.2016.08.056.

(54) Takechi-Haraya, Y.; Goda, Y.; Sakai-Kato, K. Control of Liposomal Penetration into Three-Dimensional Multicellular Tumor Spheroids by Modulating Liposomal Membrane Rigidity. *Mol Pharm* **2017**, *14* (6), 2158–2165 DOI: 10.1021/acs.molpharmaceut.7b00051.

(55) Santos, N. C.; Figueira-Coelho, J.; Martins-Silva, J.; Saldanha, C. Multidisciplinary utilization of dimethyl sulfoxide: pharmacological, cellular, and molecular aspects. *Biochem. Pharmacol.* **2003**, *65* (7), 1035–1041 DOI: 10.1016/S0006-2952(03)00002-9.

(56) Notman, R.; Noro, M.; O'Malley, B.; Anwar, J. Molecular basis for dimethylsulfoxide (DMSO) action on lipid membranes. *JACS* **2006**, *128* (43), 13982–13983 DOI: 10.1021/ja063363t.

(57) Casado, J. L.; Bañón, S. Dutrebis (lamivudine and raltegravir) for use in combination with other antiretroviral products for the treatment of HIV-1 infection. *Expert Rev Clin Pharmacol* **2015**, *8* (6), 709–718 DOI: 10.1586/17512433.2015.1090873.

(58) Ramana, L. N.; Sharma, S.; Sethuraman, S.; Ranga, U.; Krishnan, U. M. Stealth anti-CD4 conjugated immunoliposomes with dual antiretroviral drugs--modern Trojan horses to combat HIV. *Eur J Pharm Biopharm* **2015**, *89*, 300–311 DOI: 10.1016/j.ejpb.2014.11.021.

(59) Chou, T.-C. Theoretical basis, experimental design, and computerized simulation of synergism and antagonism in drug combination studies. *Pharmacol. Rev.* **2006**, *58* (3), 621–681 DOI: 10.1124/pr.58.3.10.

(60) Jiang, Y.; Cao, S.; Bright, D. K.; Bever, A. M.; Blakney, A. K.; Suydam, I. T.; Woodrow, K. A. Nanoparticle-Based ARV Drug Combinations for Synergistic Inhibition of Cell-Free and Cell-Cell HIV Transmission. *Mol Pharm* **2015**, *12* (12), 4363–4374 DOI: 10.1021/acs.molpharmaceut.5b00544.

(61) Ruttala, H. B.; Ko, Y. T. Liposomal co-delivery of curcumin and albumin/paclitaxel nanoparticle for enhanced synergistic antitumor efficacy. *Colloids Surf B Biointerfaces* **2015**, *128*, 419–426 DOI: 10.1016/j.colsurfb.2015.02.040.

(62) Meng, H.; Wang, M.; Liu, H.; Liu, X.; Situ, A.; Wu, B.; Ji, Z.; Chang, C. H.; Nel, A. E. Use of a lipid-coated mesoporous silica nanoparticle platform for synergistic gemcitabine and paclitaxel delivery to human pancreatic cancer in mice. *ACS Nano* **2015**, *9* (4), 3540–3557 DOI: 10.1021/acsnano.5b00510.

(63) Figueira, T. N.; Palermo, L. M.; Veiga, A. S.; Huey, D.; Alabi, C. A.; Santos, N. C.; Welsch, J. C.; Mathieu, C.; Horvat, B.; Niewiesk, S.; et al. In Vivo Efficacy of Measles Virus Fusion Protein-Derived Peptides Is Modulated by the Properties of Self-Assembly and Membrane Residence. *J Virol* **2016**, *91* (1), e01554 DOI: 10.1128/jvi.01554-16.

(64) Figueira, T. N.; Augusto, M. T.; Rybkina, K.; Stelitano, D.; Noval, M. G.; Harder, O. E.; Veiga, A. S.; Huey, D.; Alabi, C. A.; Biswas, S.; et al. Effective in Vivo Targeting of Influenza Virus through a Cell-Penetrating/Fusion Inhibitor Tandem Peptide Anchored to the Plasma Membrane. *Bioconjug Chem* **2018**, *29* (10), 3362–3376 DOI: 10.1021/acs.bioconjchem.8b00527.

(65) Outlaw, V. K.; Bottom-Tanzer, S.; Kreitler, D. F.; Gellman, S. H.; Porotto, M.; Moscona, A. Dual Inhibition of Human Parainfluenza Type 3 and Respiratory Syncytial Virus Infectivity with a Single Agent. *JACS* **2019**, *141* (32), 12648–12656 DOI: 10.1021/jacs.9b04615.

(66) Graham, F. L.; van der Eb, A. J. A new technique for the assay of infectivity of human adenovirus 5 DNA. *Virology* **1973**, *52* (2), 456–467.

(67) Kwon, M.; Firestein, B. L. DNA transfection: calcium phosphate method. *Methods Mol Biol* **2013**, *1018*, 107–110 DOI: 10.1007/978-1-62703-444-9_10.

(68) Reed, L. J.; Muench, H. A simple method of estimating fifty per cent endpoints. **1938**, *27*, 493–497.

(69) Derdeyn, C. A.; Decker, J. M.; Sfakianos, J. N.; Wu, X.; O'Brien, W. A.; Ratner, L.; Kappes, J. C.; Shaw, G. M.; Hunter, E. Sensitivity of human immunodeficiency virus type 1 to the fusion inhibitor T-20 is modulated by coreceptor specificity defined by the V3 loop of gp120. *J Virol* **2000**, *74* (18), 8358–8367.

(70) Mayer, L. D.; Hope, M. J.; Cullis, P. R. Vesicles of variable sizes produced by a rapid extrusion procedure. *BBA* **1986**, *858* (1), 161–168.

(71) Ladokhin, A. S.; Jayasinghe, S.; White, S. H. How to measure and analyze tryptophan fluorescence in membranes properly, and why bother? *Anal Biochem* **2000**, *285* (2), 235–245 DOI: 10.1006/abio.2000.4773.

(72) Santos, N. C.; Prieto, M. M.; Castanho, M. A. M. Interaction of the major epitope region of HIV protein gp41 with membrane model systems. A fluorescence spectroscopy study. *Biochemistry* **1998**, *37* (24), 8674–8682 DOI: 10.1021/bi9803933.

(73) Lakowicz, J. R. *Principles of Fluorescence Spectroscopy*, 3rd ed.; Springer, 2007.

(74) Fernandes, M. X.; la Torre, de, J. G.; Castanho, M. A. R. B. Joint determination by Brownian dynamics and fluorescence quenching of the in-depth location profile of biomolecules in membranes. *Anal Biochem* **2002**, *307* (1), 1–12.

(75) Coutinho, A.; Prieto, M. Ribonuclease T1 and alcohol dehydrogenase fluorescence quenching by acrylamide: A laboratory experiment for undergraduate students. *J Chem Educ* **1993**, *70* (5), 425.

(76) Koppel, D. E. Analysis of Macromolecular Polydispersity in Intensity Correlation Spectroscopy: The Method of Cumulants. *J Chem Phys* **2003**, *57* (11), 4814–4820 DOI: 10.1063/1.1678153.

(77) Provencher, S. W. CONTIN: A general purpose constrained regularization program for inverting noisy linear algebraic and integral equations. *Comput Phys Commun* **1982**, *27* (3), 229–242 DOI: 10.1016/0010-4655(82)90174-6.

(78) Provencher, S. W. A constrained regularization method for inverting data represented by linear algebraic or integral equations. *Comput Phys Commun* **1982**, *27* (3), 213–227 DOI: 10.1016/0010-4655(82)90173-4.

(79) Einstein, A. Über die von der molekularkinetischen Theorie der Wärme geforderte Bewegung von in ruhenden Flüssigkeiten suspendierten Teilchen. *Ann Phys-Berlin* **1905**, *322* (8), 549–560 DOI: 10.1002/andp.19053220806.

(80) Carvalho, P. M.; Felício, M. R.; Santos, N. C.; Gonçalves, S.; Domingues, M. M. Application of Light Scattering Techniques to Nanoparticle Characterization and Development. *Front Chem* **2018**, *6*, 237 DOI: 10.3389/fchem.2018.00237.

(81) Kaszuba, M.; Corbett, J.; Watson, F. M.; Jones, A. High-concentration zeta potential measurements using light-scattering techniques. *Philos Trans A Math Phys Eng Sci* **2010**, *368* (1927), 4439–4451 DOI: 10.1098/rsta.2010.0175.

(82) Tucker, I. M.; Corbett, J. C. W.; Fatkin, J.; Jack, R. O.; Kaszuba, M.; MacCreath, B.; McNeil-Watson, F. Laser Doppler Electrophoresis applied to colloids and surfaces. *Curr Opin Colloid In Sci* **2015**, *20* (4), 215–226 DOI: 10.1016/j.cocis.2015.07.001.

(83) Cunha-Santos, C.; Figueira, T. N.; Borrego, P.; Oliveira, S. S.; Rocha, C.; Couto, A.; Cantante, C.; Santos-Costa, Q.; Azevedo-Pereira, J. M.; Fontes, C. M. G. A.; et al. Development of synthetic light-chain antibodies as novel and potent HIV fusion inhibitors. *AIDS* **2016**, *30* (11), 1691–1701 DOI: 10.1097/QAD.0000000000001108.

(84) Chou, T.-C. Derivation and properties of Michaelis-Menten type and Hill type equations for reference ligands. *Journal of Theoretical Biology* **1976**, *59* (2), 253–276 DOI: 10.1016/0022-5193(76)90169-7.

(85) O'Brien, J.; Wilson, I.; Orton, T.; Pognan, F. Investigation of the Alamar Blue (resazurin) fluorescent dye for the assessment of mammalian cell cytotoxicity. *Eur. J. Biochem.* **2000**, *267* (17), 5421–5426.

(86) Loewe, S.; Muischnek, H. Über Kombinationswirkungen. *Archiv f. experiment. Pathol. u. Pharmakol* **1926**, *114* (5-6), 313–326 DOI: 10.1007/BF01952257.

(87) Bliss, C. I. The toxicity of poisons applied jointly. *Annals of Applied Biology* **1939**, *26* (3), 585–615 DOI: 10.1111/j.1744-7348.1939.tb06990.x.

(88) Chou, T.-C.; Talalay, P. Quantitative analysis of dose-effect relationships: the combined effects of multiple drugs or enzyme inhibitors. *Advances in Enzyme Regulation* **1984**, *22*, 27–55 DOI: 10.1016/0065-2571(84)90007-4.

Graphical Table of Contents